Biomass pyrolysis in fully-developed turbulent riser flow

S. Beetham[1], J. Capecelatro

Department of Mechanical Engineering, University of Michigan, Ann Arbor, MI 48105, USA

Abstract

This work presents a numerical study of biomass pyrolysis in turbulent riser flow. Eulerian–Lagrangian simulations of unbounded sedimenting gas-solid flows are performed to isolate the effects of particle clustering on the production of syngas and tar. This configuration provides a framework to resolve the relevant length- and time-scales associated with thermal, chemical and multiphase processes taking place in the fully-developed region of a circulating fluidized bed riser. A four-step kinetic scheme is employed to model the devolatilization of biomass particles and secondary cracking of tar. Two-way coupling between the phases leads to clusters of sand particles that generate and sustain gas-phase turbulence and transport biomass particles. Neglecting the heterogeneity caused by clusters was found to lead to a maximum over-prediction of syngas yield of 33%. Further, it was found that two-dimensional simulations over-predict the level of clustering, resulting in an under-prediction of syngas and tar yields.

Keywords: multiphase, turbulence, biomass pyrolysis, Euler-Lagrange, CFD, riser

1. Introduction

Biofuels generated from the pyrolytic upgrading of biomass are becoming a formidable alternative to fossil fuels, with the important benefits of

[1]snverner@umich.edu

Label 1	Label 2	Label 3	Label 4
A	B	C	D
E	F	G	H

Table 1: This is a caption.

sustainability, carbon neutrality and economic feasibility [1, 2, 3, 4]. The catalytic upgrading of biomass solids (e.g. cellulose-based materials often originating from agricultural waste) to useful products such as syngas, typically occurs in the riser of a circulating fluidized bed reactor. While such technologies show great promise in a laboratory setting, scale-up to commercial application remains a key hurdle [5]. A recurring challenge is the need to ensure optimal contact between the reacting flow and fluidized particles (e.g. catalysts and biomass). While there has been significant progress characterizing hydrodynamic interactions in particle-laden flows [6], much less is known about interphase heat and mass transfer.

2. Methodology

2.1. System description

The simulation configuration considered in the present study is designed to provide a model flow that captures key phenomenology in the reactor. We focus on what would be considered the fully-developed region of the riser. Assuming the flow is sufficiently far from the entrance, the two phases would evolve spatially upward without retaining memory of any entrance effects. If we further assume the simulation domain is far from the walls of the riser, and given that the flow equations are frame invariant, we can consider a temporally-developing frame of reference in an unbounded system. Focusing on the fully-developed region of the riser flow enables us to resolve a broader range of length- and time-scales associated with biomass pyrolysis than could otherwise be achieved. Further, the present configuration isolates the role of multiphase dynamics on production yield.

Very simple table:

2.2. Chemical kinetics

During catalytic upgrading, biomass particles are decomposed into char, syngas and tar vapor. The tar vapor undergoes secondary cracking to form additional syngas. In the current study, this process is modeled by four

Physical properties					
			biomass	*sand*	*char*
d_p	[µm]	Particle diameter	500	200	
ρ_p	[kg/m^3]	Particle density[7]	400	2649	2333
$C_{p,p}$	[J/kg K]	Particle heat capacity[8]	2300	800	1100
T_p^0	[K]	Initial particle temperature	300	790	
κ_p	[J/m s K]	Particle thermal conductivity[8]	0.3	0.27	1
			N_2	*tar*	*syngas*
ρ_g	[kg/m^3]	Fluid density	EOS[1]	EOS[1]	EOS[1]
$C_{p,g}$	[J/kg K]	Fluid heat capacity[8]	1121	2500	1100
T_g^0	[K]	Initial fluid temperature	790	–	–
κ_g	[J/m s K]	Fluid thermal conductivity[8]	5.63×10^{-2}	2.57×10^{-2}	
ν_g	[m^2/s]	Fluid kinematic viscosity	[9]	$3\times10^{-5}\rho_g$ [8]	

Dimensional parameters				
			biomass	*sand*
τ_p	[s]	Particle response time	0.15	0.16
$\mathcal{L}$	[m]	Cluster length	0.004	0.005
$\mathcal{V}$	[m/s]	Terminal velocity	0.028	0.0297
$\boldsymbol{g}$	[m/s^2]	Gravity	$(-0.18, 0, 0)$	

Non-dimensional parameters			
		biomass	*sand*
$\langle\varepsilon_p\rangle$	Mean particle volume fraction	0.005	0.01
N_p	Number of particles	17 302	540 710
Φ_m	Mass loading	4.74	62.8
Re	Reynolds number	1.46	1.74
Fr	Froude number	8.71	24.4
Ar	Archimedes number	3.01	1.28

Table 2: Summary of relevant simulation parameters. [1] Equation of state for an ideal gas (Eq. **??**). Note all biomass quantities are given at the unreacted state (i.e. at $t = t^\star$).

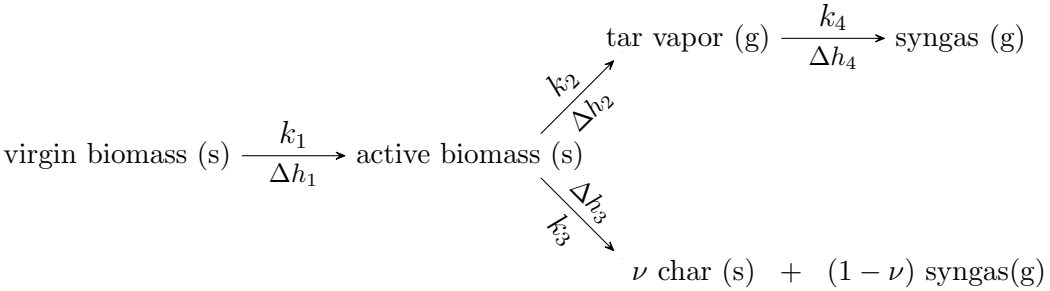

Figure 1: Kinetic scheme used in the present work. Solid biomass consists of cellulose, hemicellulose and lignin. The phase of each constituent is noted in parentheses. The heats of formation for each reaction are given by: $\Delta h_1 = 0$ [12], $\Delta h_2 = 255$ kJ/kg [13], $\Delta h_3 = -20$ kJ/kg [13], and $\Delta h_4 = -42$ kJ/kg [14].

irreversible, first-order reactions commonly used in the literature [10, 11]. A summary of the kinetic scheme is shown in Fig. 1. Here, solid biomass is composed of three components: cellulose, hemicellulose and lignin. The biomass under consideration in this study is bagasse, the woody pulp by-product resultant of the commercial processing of sugarcane. The species composition of bagasse is given as

$$\text{Biomass} = \alpha\text{Cellulose} + \beta\text{Hemicellulose} + \gamma\text{Lignin}, \tag{1}$$

where the initial composition is given by $(\alpha, \beta, \gamma) = (0.36, 0.47, 0.17)$ [10].

Upon heating, virgin biomass is activated and then devolatized into char, tar and syngas. Char remains within the particle while tar and syngas are transferred to the gas phase. The mass rates of change for the species involved in the activation and devolatization of biomass particles are given by

$$\frac{dm_i^v}{dt} = -k_{1_i} m_i^v \tag{2}$$

$$\frac{dm_i^a}{dt} = k_{1_i} m_i^v - (k_{2_i} + k_{3_i}) m_i^a \tag{3}$$

$$\frac{dm_{\text{char}}}{dt} = \sum_i \nu_i k_{3_i} m_i^a \tag{4}$$

$$\frac{dm_{\text{tar}}}{dt} = \sum_i k_{2_i} m_i^a \tag{5}$$

$$\frac{dm_{\text{syn}}}{dt} = \sum_i (1-\nu_i) k_{3_i} m_i^a \tag{6}$$

Constituent	Reaction	ν (k_3)	A (s^{-1})	E (MJ/kmol)
Cellulose [15]	k_{1c}	-	2.8×10^{19}	242.4
	k_{2c}	-	3.28×10^{14}	196.5
	k_{3c}	(ν_c) 0.35	1.3×10^{10}	150.5
Hemicellulose [16]	k_{1h}	-	2.1×10^{16}	186.7
	k_{2h}	-	8.75×10^{15}	202.4
	k_{3h}	(ν_h) 0.60	2.6×10^{11}	145.7
Lignin[16]	k_{1l}	-	9.6×10^{8}	107.6
	k_{2l}	-	1.5×10^{9}	143.8
	k_{3l}	(ν_l) 0.75	7.7×10^{6}	111.4
Tar [17]	k_4	-	4.25×10^{6}	108.0

Table 3: Rate coefficients used in the Arrhenius reaction (8).

where $i = c, h, l$ corresponds to the biomass species cellulose, hemicellulose and lignin and the superscripts a and v refer to activated and virgin biomass, respectively. Secondary cracking, as it is a homogeneous reaction in the gas phase, is solved exclusively on the Eulerian mesh. Since the biomass particles are composed at any point in time of virgin biomass, active biomass and char, the previous equations allow for an expression for the total rate of mass change for a biomass particle to be written as

$$\frac{dm_{\text{bio}}}{dt} = \sum_i \frac{dm_i^v}{dt} + \sum_i \frac{dm_i^a}{dt} + \frac{dm_{\text{char}}}{dt}. \tag{7}$$

Reaction rates for the kinetics are dictated by the Arrhenius equation

$$k_i = A_i \exp[-E_i/RT_p] \tag{8}$$

where A_i is the pre-exponential factor, E_i is the activation energy, R is the gas constant, and T_p is the particle temperature. These quantities are summarized in Table 3. Chemical kinetics are treated on the scale of the particle, and as such the mass of each species contained within each particle is tracked, but the transport within the particle itself is not considered.

2.3. Gas-phase description

The gaseous phase initially consists of pure nitrogen and evolves into a mixture of nitrogen, gaseous tar and syngas. To enforce conservation of

mass, momentum and energy in the presence of solid particles, we consider the volume-filtered Navier–Stokes equations [18, 19]. Conservation of mass is given by

$$\frac{\partial}{\partial t}(\varepsilon_g \rho_g) + \nabla \cdot (\varepsilon_g \rho_g \boldsymbol{u}_g) = \sum_{l=1}^{2} \dot{\mathcal{M}}_l \tag{9}$$

where $\boldsymbol{u}_g = [u_g, v_g, w_g]^{\mathrm{T}}$ is the fluid velocity and $\mathcal{M}_l$ is the interphase mass source term, with $l = (\mathrm{tar}, \mathrm{syn})$, referring to the reactive species, tar and syngas, respectively. Conservation of momentum is given by

$$\frac{\partial}{\partial t}(\varepsilon_g \rho_g \boldsymbol{u}_g) + \nabla \cdot (\varepsilon_g \rho_g \boldsymbol{u}_g \boldsymbol{u}_g) = \varepsilon_g \nabla \cdot \boldsymbol{\tau}_g + \varepsilon_g \rho_g \boldsymbol{g} + \mathcal{F} + \boldsymbol{F}_{\mathrm{mfr}} \tag{10}$$

where $\mathcal{F}$ accounts for two-way coupling between the gas and solid phases, which will be made explicit in Sec. 2.3. $\boldsymbol{F}_{\mathrm{mfr}}$ is a source term used to ensure that the system maintains a constant mass flow rate in order to achieve a statistically stationary state. The viscous stress tensor is given by

$$\boldsymbol{\tau}_g = -p_g \mathbb{I} + \mu_g^* \left[\nabla \boldsymbol{u}_g + \nabla \boldsymbol{u}_g^{\mathrm{T}} - \frac{2}{3} (\nabla \cdot \boldsymbol{u}_g) \mathbb{I} \right], \tag{11}$$

where p_g is the gas-phase pressure, $\mathbb{I}$ is the identity matrix and μ_g^* is an effective viscosity accounting for enhanced dissipation at the particle scale, given by [20]

$$\mu_g^* = \mu_g \varepsilon_g^{-2.8}. \tag{12}$$

Figure 2 shows the evolution of Favre averaged temperature, syngas mass fraction and tar mass fraction. Here, Favre average quantities are defined as $\widetilde{(\cdot)} = \langle \varepsilon_g \rho_g (\cdot) \rangle / \langle \varepsilon_g \rho_g \rangle$. To assess the role of heterogeneity caused by clusters on thermochemical conversion, comparisons are made against a zero-dimensional system that models a homogeneous flow under identical conditions. In this system, all spatial variations are neglected and variables are solved for as a function of time only. A single, stationary biomass particle is introduced at a starting temperature of 300 K into a hot volume of nitrogen such that the volume fraction $\langle \varepsilon_p \rangle$ is consistent with the three-dimensional simulation. As was done in the three-dimensional case, the mean gas-phase temperature is forced to remain constant at 790 K.

Three key observations can be made: (1) spatial variations present in CIT induce variations in gas-phase temperature (which are large at early times due to the discrepancy in initial temperature between biomass particles and

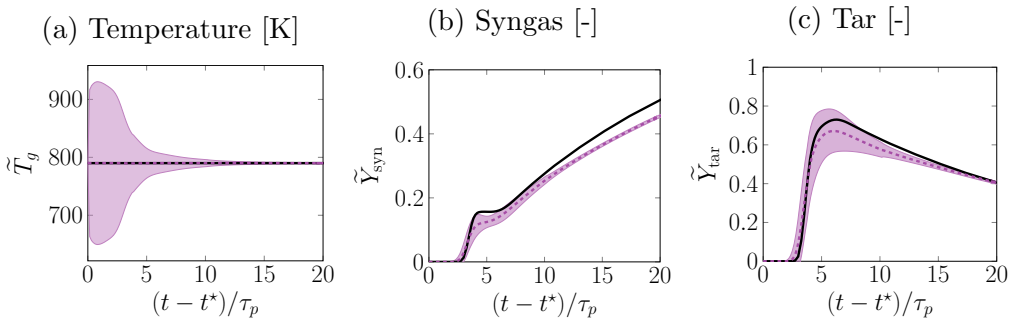

Figure 2: Evolution of the gas-phase temperature, syngas, and tar. Mean values for three-dimensional CIT (dashed purple lines) and a homogeneous (zero-dimensional) system under identical conditions (solid black lines). The shaded regions correspond to ± 3 times the standard deviation in CIT.

their surroundings). (2) Variations also exist in the mass fractions of tar and syngas. At early times ($t \lessapprox 4\tau_p$), syngas and tar are predominantly formed in clusters where the majority of biomass particles exist, despite the lower temperature in these regions. The species are then transported away from clusters, where secondary reactions occur. (3) Because the zero-dimensional model does not account for heterogeneity in spatial distribution, it over-predicts both tar and syngas formation. The typical residence time for cellulosic biomass in a circulating fluidized bed reactor is approximately 1 s, corresponding to $6.25\tau_p$. Figure 2 shows that the zero-dimensional model over-predicts both tar and syngas production when simulation time reaches standard residence time by 8.9% and 13.0%, respectively. It is notable that for residence times less than 1 s, the zero-dimensional model achieves a maximum over-prediction of 32.9% for syngas yield at $(t - t^\star)/\tau_p = 4.02$ (0.64 s). Maximum over-prediction in the yield of tar is 9.0% occurring at $(t - t^\star)/\tau_p = 4.63$ (0.74 s). This suggests that heterogeneity plays an especially important role in systems with short residence times, for instance flash pyrolysis.

References

[1] M. M. Write, J. A. Satrio, R. C. Brown, D. E. Daugaard, and D. D. Hsu. Techno-economic analysis of biomass fast pyrolysis to transportation fuels. *NREL Technical Report*, NREL/TP-6A20-46586, 2010.

[2] M. S. Mettler, D. G. Vlachos, and P. J. Dauenhauer. Top ten fundamen-

tal challenges of biomass pyrolysis for biofuels. *Energy & Environmental Science*, 5:7797–7809, 2012.

[3] A. V. Bridgwater. Review of fast pyrolysis of biomass and product upgrading. *Biomass and Bioenergy*, 38:68–94, 2012.

[4] A. E. Farrell, R. J. Plevin, B. T. Turner, A. D Jones, M. O'Hare, and D. M. Kammen. Ethanol can contribute to energy and environmental goals. *Science*, 311:506–508, 2006.

[5] M. P. Dudukovic. Frontiers in reactor engineering. *Science*, 325(5941): 698–701, 2009.

[6] S. Balachandar and J. K. Eaton. Turbulent dispersed multiphase flow. *Annual Review Fluid Mechanics*, 42:111–133, 2010.

[7] R.C. Brown. Biorenewable resources: Engineering new products from agriculture. *Iowa State Press: Ames, IA*, 2003.

[8] D. Lathouwers and J. Bellan. Yield optimization and scaling of fluidized beds for tar production from biomass. *Energy Fuels*, 15:1247–1262, 2001.

[9] E.W. Lemmon and R.T. Jacobsen. Viscosity and thermal conductivity equations for nitrogen, oxygen, argon and air. *International Journal of Thermophysics*, 25(1):21–69, 2004.

[10] X. Xue, T.J. Heindel, and R.O. Fox. A CFD model for biomass fast pyrolysis in fluidized-bed reactors. *Chemical Engineering Science*, 66: 2440–2452, 2011.

[11] Q. Xiong, S.K. Kong, and A. Passalacqua. Development of a generalized numerical framework for simulating biomass fast pyrolysis in fluidized-bed reactors. *Chemical Engineering Science*, 99:305–313, 2013.

[12] C. Di Blasi. Numerical simulation of cellulose pyrolysis. *Biomass and Bioenergy*, 7:87–98, 1994.

[13] C.A. Koufopanosi, N. Papayannakos, G. Maschio, and A. Lucchesi. Modelling of the pyrolysis of biomass particles. studies on kinetics, thermal and heat transfer effects. *The Canadian Journal of Chemical Engineering*, 69:907–915, 1991.

[14] L.J. Curtis and D.J Miller. Transport model with radiative heat transfer for rapid cellulose pyrolysis. *Industrial & Engineering Chemistry Research*, 27:1775–1783, 1988.

[15] A.G.W. Bradbury, Y. Sakai, and F. Shafizadeh. A kinetic model for pyrolysis of cellulose. *Journal of Applied Polymer Science*, 23:3271–3280, 1979.

[16] R.S. Miller and J. Bellan. A generalized biomass pyrolysis model based on superimposed cellulose, hemicellulose, and lignin kinetics. *Combustion Science and Technology*, 126:97–138, 1997.

[17] A.G. Liden, F. Berruti, and D.S. Scott. A kinetic model for the production of liquids from the flash pyrolysis of biomass. *Chemical Engineering Communications*, 65, 1988.

[18] T.B. Anderson and R. Jackson. Fluid mechanical description of fluidized beds. Equations of motion. *Industrial & Engineering Chemistry Fundamentals*, 6(4):527–539, 1967.

[19] J. Capecelatro and O. Desjardins. An Euler–Lagrange strategy for simulating particle-laden flows. *Journal of Computational Physics*, 238:1–31, 2013.

[20] L.G. Gibilaro, K. Gallucci, R. Di Felice, and P. Pagliai. On the apparent viscosity of a fluidized bed. *Chemical Engineering Science*, 62(1-2):294–300, 2007.